Journal of Power Sources 189 (2009) 269–278

Contents lists available at ScienceDirect

Journal of Power Sources

journal homepage: www.elsevier.com/locate/jpowsour

Dependence of property, crystal structure and electrode characteristics on Li content for $Li_xNi_{0.8}Co_{0.2}O_2$ as a cathode active material for Li secondary battery

Yasushi Idemoto*, Yu Takanashi, Naoto Kitamura

Department of Pure and Applied Chemistry, Faculty of Science & Technology, Tokyo University of Science, 2641 Yamazaki, Noda-shi, Chiba 278-8510, Japan

ARTICLE INFO

Article history:
Received 27 June 2008
Received in revised form
12 September 2008
Accepted 15 September 2008
Available online 24 September 2008

Keywords:
Lithium secondary battery
Cathode material
Crystal structure
Layered structure
Lithium content

ABSTRACT

We investigated the dependence of the properties, crystal and electronic structures and electrode characteristics of $Li_xNi_{0.8}Co_{0.2}O_2$ as a cathode active material for Li secondary batteries. $Li_xNi_{0.8}Co_{0.2}O_2$ was prepared by a solid-state method and solution method. The crystal structure was determined by neutron and X-ray diffractions using the Rietveld analysis. All the samples were obtained as the α-$NaFeO_2$ type with the space group *R*-3*m*. From the charge–discharge test, the cycle performance was improved with the decreasing Li content ($x \leqq 1.066$) although the discharge capacity decreased. Samples made by the solid-state method showed a better electrode performance than those made by the solution method. We measured the chemical diffusion coefficient of Li ($\widetilde{D}_{Li^+}$) by the GITT method. The $\widetilde{D}_{Li^+}$ in the stable cycle region was much improved in the sample prepared by the solid-state method than by the solution method. From the neutron powder diffraction, it was confirmed that Li_2CO_3 was formed by increasing the Li content ($0.994 < x \leqq 1.066$) as a secondary phase. Cation mixing was improved with the decreasing Li content. The bond length of the 3b site–6c site decreased with decreasing Li content. From the electron density images on the (1 1 0) plane for $Li_xNi_{0.8}Co_{0.2}O_2$, the covalent bond of the 3b site–6c site increased with the decreasing Li content. This may be one of the reasons why the cycle performance improved with the decreasing Li content.

1. Introduction

$LiCoO_2$-derived materials are presently the most widely used cathode active material for commercial lithium-ion rechargeable battery electrodes. However, because they contain the rare metal Co, they have associated costs and environmental problems. A search for alternative materials is currently underway [1]. In our laboratory, we have investigated the properties, crystal structure, thermodynamic stability, and battery performances of $Li_xMn_{2-y}M_yO_4$ (M = Li, Mg, Zn, Ni, Co), $Li_xMn_{1-y}M_yO_2$ (M = Al, Cu), and $Li_x(Mn,Co,Ni,M)O_2$ (M = Al, Ti, Fe) [2–6]. The results show that when the lithium composition of $Li_xMn_{1/3}Co_{1/3}Ni_{1/3}O_2$, which has a layered structure, is increased, the discharge capacity increases, and hence the synthesis method influences the battery properties [5,6]. We also clarified that the structural stability, thermodynamic stability, and electrical properties of the material are correlated [5,6]. Recently, Li(Ni, Co)O_2, which has the same layered structure as $Li_xMn_{1/3}Co_{1/3}Ni_{1/3}O_2$, has been gaining attention as a promising alternative to $LiCoO_2$. It can be synthesized relatively easily and has a higher discharge capacity than $LiCoO_2$. Li(Ni, Co)O_2 has been synthesized by a variety of methods and it is known that its solid-state properties and battery performances differ depending on the method of synthesis [7–9]. In general however, in Li–Ni–Co–O type oxides during high-temperature firing, if the Li composition is insufficient, Ni^{2+}, which has nearly the same ionic radius as Li^+, contaminates the empty sites formed due to Li deficiency, and the nonstoichiometric composition $[Li_d{}^+Ni_{1-d}{}^{2+}]_{3a}\ [Ni_{1-d}{}^{2+}Ni_{d(2-x)-2(1-x)}{}^{3+}Co_{(1-x)(2-d)}{}^{3+}]_{3b}O_2{}^{2-}$ is generated. The areas in which Ni has contaminated the 3a site are regarded as local NiO disordered array halite layers (space group: *Fm*-3*m*), which obstruct the battery reaction [7].

In this study we synthesized $Li_xNi_{0.8}Co_{0.2}O_2$ with different Li compositions ($0.965 \leq x \leq 1.111$) by two methods, a solid-state method and a solution method, and evaluated the solid-state properties and battery performances. We also made powder neutron diffraction and X-ray diffraction measurements and performed crystal structure analysis based on the Rietveld method and investigated the nuclear and electron density distributions based on the maximum entropy method (MEM). We studied the influence of the synthesis method and Li composition on the solid-state properties, structure, and battery performances. In addition, we performed structural analysis of chemically delithiated specimens and inves-

* Corresponding author. Tel.: +81 4 7122 9493; fax: +81 4 7123 9890.
E-mail address: idemoto@rs.noda.tus.ac.jp (Y. Idemoto).

0378-7753/$ – see front matter © 2008 Elsevier B.V. All rights reserved.
doi:10.1016/j.jpowsour.2008.09.048

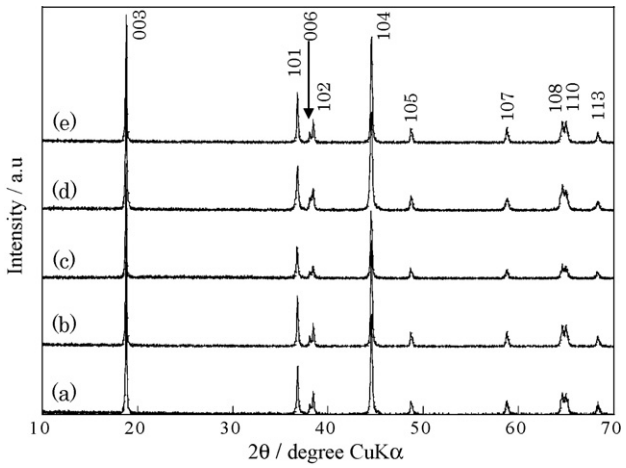

Fig. 1. Powder X-ray diffraction patterns of $Li_xNi_{0.8}Co_{0.2}O_2$ prepared by solid-state method. (a) $x = 0.965$, (b) $x = 0.994$, (c) $x = 1.041$, (d) $x = 1.066$, and (e) $x = 1.111$.

tigated the relationship between the charge and discharge process and the crystal structure.

2. Experimental

For samples synthesized by the solid-state method, $LiOH{\cdot}H_2O$ (99.9%, Wako Pure Chemical Industries, Ltd.), $Ni(OH)_2$ (99.9%, Wako Pure Chemical Industries, Ltd.), and CoO (99.9%, Soekawa Chemical Co.) were used as the starting materials. $LiOH{\cdot}H_2O$ was in 5% excess of the nominal composition. The mixture were ground in an agate mortar for 15 h and then pressed into pellets. These pellets were then heated at 600 °C for 15 h in air and then ground into a powder. This powder was again pressed into pellets (40 MPa), then calcined at 800 °C for 15 h in air, then rapidly cooled to room temperature. For the solution method (citrate precursors method), $LiCH_3COO{\cdot}2H_2O$ (99%, Soekawa Chemical Co.), $Ni(CH_3COO)_2{\cdot}4H_2O$ (99%, Soekawa Chemical Co.), and $Co(CH_3COO)_2{\cdot}4H_2O$ (99%, Soekawa Chemical Co.) were dissolved in distilled water and mixed with an aqueous solution of citric acid (as a chelating agent and same weight of $LiCH_3COO{\cdot}2H_2O$). $LiCH_3COO{\cdot}2H_2O$ was in 5% excess of the nominal composition. The solutions were heated at 130 °C for 24 h in air to obtain dry precursors. The precursor was then heated at 600 °C for 15 h in air and then pressed into pellets (40 MPa). Next, it was calcined at 800 °C for 15 h in air, then rapidly cooled to room temperature. To obtain solid-state samples with lower Li contents ($x < 0.965$), a Li^+ extraction was carried out in a batch process by immersing the pellet in a 0.5 mol dm^{-3} $(NH_4)_2S_2O_8$ solution for different times under ambient conditions [10].

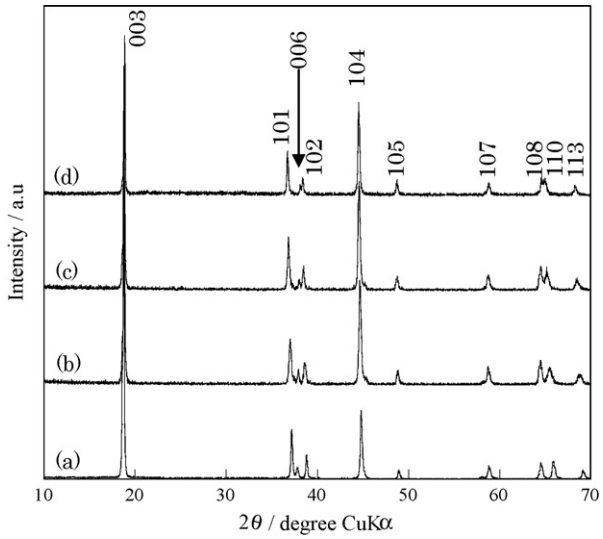

Fig. 2. Powder X-ray diffraction patterns after chemical delithiation for $Li_xNi_{0.8}Co_{0.2}O_2$ prepared by solid-state method. (a) $x = 0.530$, (b) $x = 0.660$, (c) $x = 0.756$, and (d) $x = 0.994$.

Table 1
Lattice constant of $Li_xNi_{0.8}Co_{0.2}O_2$ prepared by various synthetic methods.

Synthetic method	Li content, x	a (nm)	c (nm)
Solid-state method	0.530	0.28344(4)	1.4283(3)
	0.660	0.28507(7)	1.4205(6)
	0.756	0.2861(1)	1.424(9)
	0.965	0.2869(7)	1.419(6)
	0.994	0.2868(2)	1.418(3)
	1.041	0.2868(4)	1.420(4)
	1.066	0.2864(7)	1.415(5)
	1.111	0.2868(5)	1.418(4)
Solution method	0.651	0.28453(7)	1.4305(6)
	0.880	0.28649(6)	1.4213(5)
	0.974	0.2873(1)	1.420(1)
	0.996	0.2871(5)	1.422(2)
	1.082	0.2868(5)	1.419(4)

The obtained samples were characterized by powder XRD (Philips, X'Pert Pro). The composition of the metal components was analyzed by inductive coupled plasma spectrometry (Shimadzu Co., ICPS-750). The crystal structure of the obtained sample was studied by powder neutron diffraction using HERMES [11] of IMR at JRR-3M in JAERI. The data were refined by the Rietveld technique using the Rietan-2000 program [12]. The bond lengths were calculated by the program ORFEE [12] component of Rietan-2000. The bond valence sum [13] was calculated by the VICS program [14]. The nuclear densities analyzed by powder neutron diffraction and the electron densities by powder X-ray diffraction were calculated by the maximum entropy method (MEM) using the PRIMA program [15].

The electrochemical characterization was carried out using HS-cells (Hosen Co.). The cell was composed of the obtained sample as the working electrode, a lithium metal anode as the counter electrode and a polypropylene separator. The cathode was prepared by mixing a 92:4:4 (w/w) ratio of the active materials, acetylene black, and polyvinylidene fluoride binder, respectively, in N-methyl pyrro-

Table 2
Analytical composition of $Li_xNi_{0.8}Co_{0.2}O_2$ prepared by various synthetic methods.

Synthetic method	Li content, x	Li	Ni	Co
Solid-state method	0.530	0.530(5)	0.784(5)	0.216(1)
	0.660	0.6600(6)	0.7954(5)	0.2046(3)
	0.756	0.756(1)	0.7930(7)	0.2069(4)
	0.965	0.965(2)	0.805(6)	0.195(3)
	0.994	0.994(2)	0.798(1)	0.202(3)
	1.041	1.041(1)	0.765(2)	0.194(9)
	1.066	1.066(2)	0.740(5)	0.194(4)
	1.111	1.111(8)	0.687(4)	0.202(6)
Solution method	0.438	0.438(2)	0.803(2)	0.197(2)
	0.651	0.651(2)	0.805(2)	0.195(3)
	0.880	0.880(2)	0.806(2)	0.194(5)
	0.974	0.974(5)	0.803(9)	0.197(4)
	0.996	0.996(1)	0.807(2)	0.197(1)
	1.082	1.082(1)	0.734(1)	0.184(2)

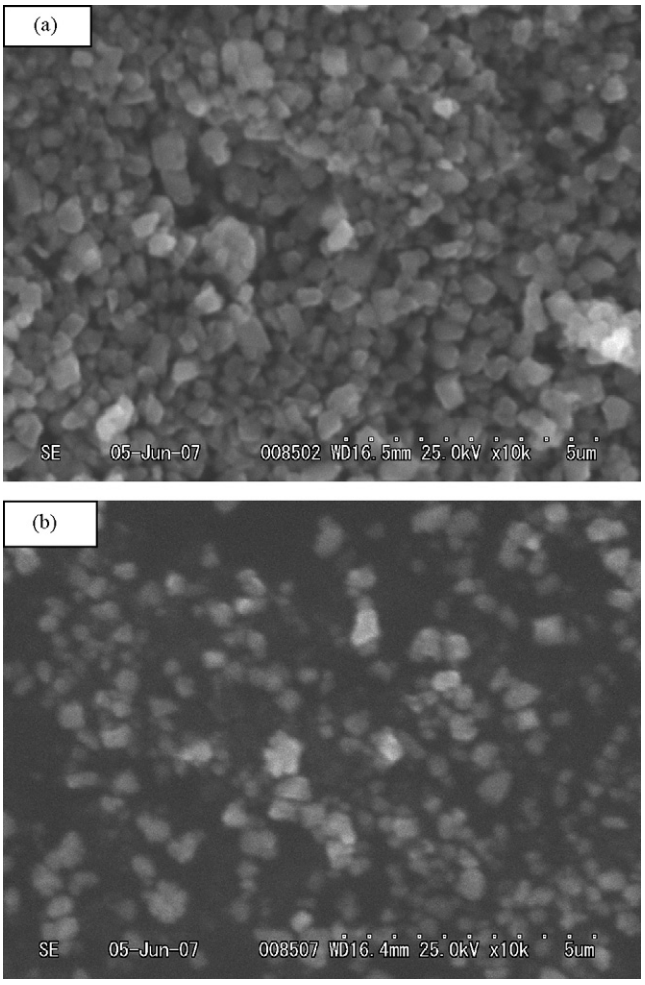

Fig. 3. SEM photographs of $LiNi_{0.8}Co_{0.2}O_2$ particle. (a) solid-state method and (b) solution method.

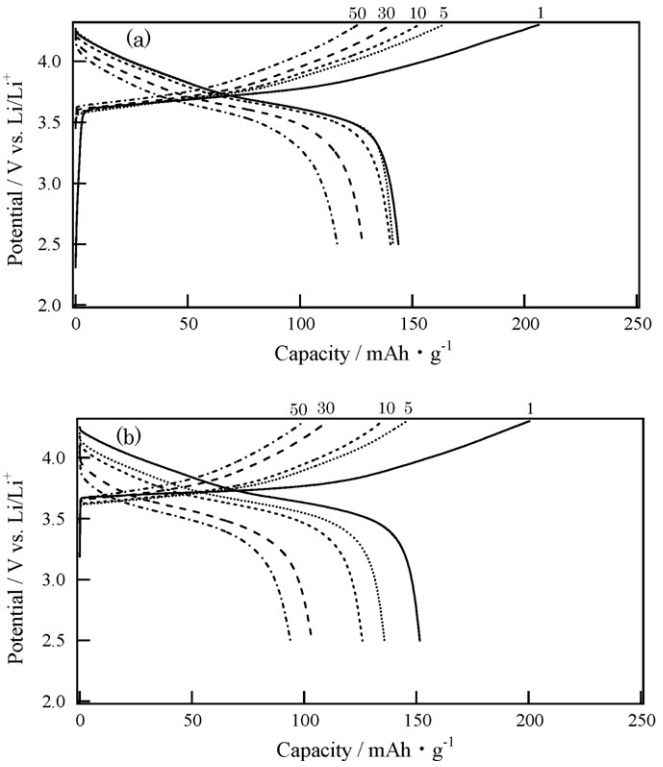

Fig. 4. Charge–discharge curves of $LiNi_{0.8}Co_{0.2}O_2$ (temperature: 25 °C, current density: 0.2 mA cm^{-2}, cut-off voltage: 2.5–4.3 V vs. Li/Li^+): (-·-·-·-) 50th: (– – –) 30th: (—·—) 10th: (·····) 5nd: (—) 1st. (a) solid-state method and (b) solution method.

lidinone. The resulting paste was applied to an aluminum current collector and the electrodes were dried at 150 °C in a vacuum, then pressed at 40 MPa. The electrolyte was a solution of 1.0 M $LiPF_6$ dissolved in a 1:2 (volume) mixture of ethylene carbonate (EC)/diethyl carbonate (DEC) (Kishida Chemical, Ltd.). All procedures were performed in an argon-filled glove box.

The electrode characteristics of the obtained samples were characterized by cyclic voltammetry (Hokuto Denko Co., HZ-3000) and charge–discharge tests (Hokuto Denko Co., SM8 V.16). The chemical diffusion coefficient of Li^+ for $Li_xNi_{0.8}Co_{0.2}O_2$ at the 3rd cycle was investigated by the GITT method [16].

3. Results and discussion

3.1. Sample characterization

Fig. 1 shows example XRD patterns of samples made using the solid-state method and Fig. 2 shows example XRD patterns of chemically delithinated $Li_xNi_{0.8}Co_{0.2}O_2$ samples made using the solid-state method. Fig. 1 shows that *R*-3*m* ascription was achieved at the space group in all synthesized samples. In addition, the clear splitting of the (0 0 6)–(1 0 2) and (1 0 8)–(1 1 0) doublet peaks suggest it has a layered structure [17]. Furthermore, Fig. 2 shows that the layered structure is preserved in chemical delithinated samples.

For samples containing Ni, it is possible that cation mixing occurs; Ni^{2+} has nearly the same ionic radius as Li^+ and can contaminate a Li site, while Li^+ can contaminate a Ni^{2+} site. The specified index requires that the relative intensity rate of the (0 0 3) and (1 0 4) peaks [R=(0 0 3)/(1 0 4)] be at least 1.2 [18]. The R value was 1.2 or more for all samples, confirming that samples with some cation mixing were obtained. Quantitative details regarding cation mixing are given in Section 3.4.

Table 1 shows the lattice constants of samples synthesized using both methods. The Li composition was determined by composition analysis. In samples with excessively high Li composition, no large change is seen in the lattice constant. However, in samples made by either method that have had Li chemically removed, there is a tendency for the lattice parameter a to decrease and the lattice parameter c to increase as the Li composition decreases. It is assumed that Li desorption increases the valence of Ni in the constituent layers, a decrease in the ionic radius causes the lattice parameters a and b to decrease. However, an increase in the electrostatic repulsion between oxygen ions in the different layers causes the lattice parameter c to increase. Table 2 shows the composition ratio of the metallic constituents for samples synthesized using both methods. For samples with decreased Li, the composition ratio was calculated taking the total metal constituent composition at the 3b site as 1. For samples with Li composition of 1 or greater, the composition ratio was calculated taking the total metal constituent composition as 2. We found that because the analytical composition value was extremely close to the nominal composition, samples with well controlled composition ratios were obtained. Fig. 3 shows scanning electron micrograph (SEM) photos of samples

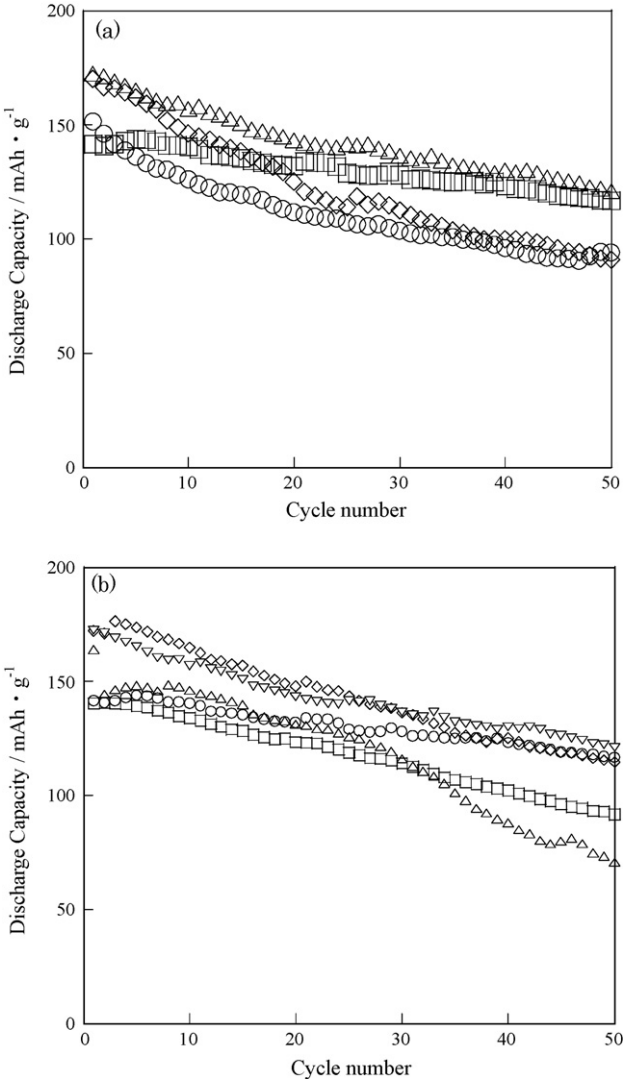

Fig. 5. Cycle performances of $Li_xNi_{0.8}Co_{0.2}O_2$. (Temperature: 25 °C, Current density: 0.2 mA cm^{-2}, cut-off voltage: 2.5–4.3 V vs. Li/Li$^+$) ○: x = 0.974 (solution method), □: x = 0.965 (solid-state method) ◊: x = 1.082 (solution method), △: x = 1.066 (solid-state method). (a) ○: x = 0.974 (solution method), □: x = 0.965 (solid-state method) ◊: x = 1.082 (solution method), △: x = 1.066 (solid-state method). ○: x = 0.965, □: x = 0.994, ◊:x = 1.041, △: x = 1.066, ▽:x = 1.11 (solid-state method). (b) ○ x = 0.965, □: x = 0.994, ◊:x = 1.041, △: x = 1.066, ▽:x = 1.11 (solid-state method).

synthesized using both methods. The particles were sufficiently small with diameters of about 0.5 μm; no differences in particle radius and particle shape due to the synthesis method could be seen.

3.2. Electrode properties

The charge–discharge curves of $Li_xNi_{0.8}Co_{0.2}O_2$ synthesized using both methods are shown in Fig. 4. Charging and discharging takes place around 4 V, i.e., it is a 4 V level battery. In addition, in each sample the irreversible capacity of the first cycle is large, greater than that of the second cycle and after second cycle is improved. In the first cycle, the irreversible capacity can be ascribed to the formation of a solid electrolyte interface (SEI) [19]. The cycling performances of each of the samples obtained are shown in Fig. 5. Fig. 5(a) clearly shows that samples synthesized using the solid-state method have better cycling performances than solution method samples. Fig. 5(b) shows the cycling performances for $Li_xNi_{0.8}Co_{0.2}O_2$, for which the Li composition was changed during synthesis using the solid-state method. This shows that decreasing the Li composition decreases the first discharge capacity while increasing the discharge capacity maintenance ratio and improving the cycling performance. The factors behind this are carefully investigated in Section 3.4 from the perspective of crystal structure.

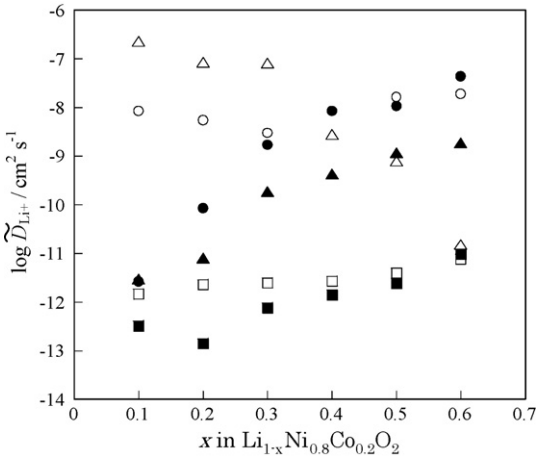

Fig. 6. Chemical diffusion coefficient of Li$^+$ of $Li_{0.965}Ni_{0.8}Co_{0.2}O_2$ (charge ○, discharge ●), and $Li_{1.041}Ni_{0.8}Co_{0.2}O_2$ (charge □, disharge ■) prepared by solid-state method and $Li_{0.974}Ni_{0.8}Co_{0.2}O_2$ (charge △, disharge ▲) prepared by solution method.

3.3. Investigation of the chemical diffusion coefficient by the GITT method

As mentioned earlier, differences are seen in the cycle performance of $Li_xNi_{0.8}Co_{0.2}O_2$ depending on the synthesis method and Li composition. In $LiCoO_2$, $LiNiO_2$, $LiMn_2O_4$, $LiMn_{1/2}Ni_{1/2}O_2$, and $LiMn_{1/3}Co_{1/3}Ni_{1/3}O_2$, which have the same layered structure, a direct correlation is seen between the Li$^+$ chemical diffusion coefficient and battery performances [20–24]. Therefore, in this study, we assessed the Li$^+$ chemical diffusion coefficient in the third cycle where the charge–discharge characteristics were quantified. There are various ways to measure the chemical diffusion coefficient, such as the GITT method [25], the PITT method [26], and the impedance method [27]. In this study, the GITT method (constant current intermittent titration) was used to measure the chemical diffusion coefficient of $Li_xNi_{0.8}Co_{0.2}O_2$. Fig. 6 shows the Li$^+$ chemical diffusion coefficient for each sample calculated using the GITT method. The fact that the chemical diffusion coefficient changed continuously with respect to the Li composition for all samples suggests that

Table 3
Final results of Rietveld refinements for $Li_{0.994}Ni_{0.8}Co_{0.2}O_2$ synthesized by solid-state method in space group R-3m at room temperature. B is isotropic thermal parameters. Numbers in parentheses are estimated standard deviations of the last significant digit, and parameters without deviations are fixed.

Atom	Site	x	y	z	$10^2 \times B$ (nm^2)	Site occupancy
Li	3a	0	0	0	0.3(1)	0.968
Ni	3a	0	0	0	0.3(1)	0.032(4)
Li	3b	0	0	1/2	0.39(4)	0.026
Ni	3b	0	0	1/2	0.39(4)	0.766
Co	3b	0	0	1/2	0.39(4)	0.202
O	6c	0	0	0.2413(1)	0.50(5)	1

R-factors are R_{wp} = 7.78%, R_p = 5.80%, R_{exp} = 5.92%, S = 1.31, a = 0.287002(7) nm, c = 1.41851(2) nm.

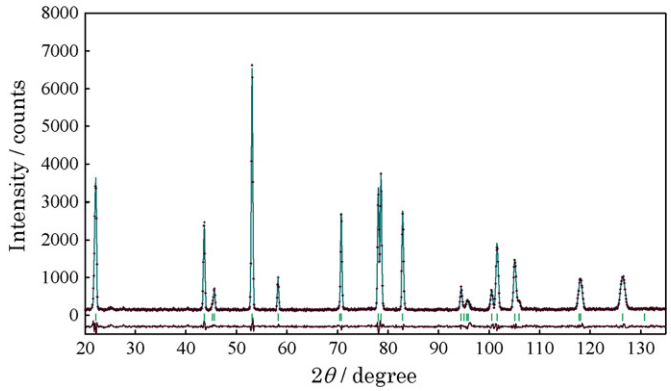

Fig. 7. Rietveld refinement patterns of $Li_{0.994}Ni_{0.8}Co_{0.2}O_2$ synthesized by solid-state method. Plus marks show observed neutron diffraction intensities and a solid line represents calculated intensities. The vertical marks below the patterns indicate the positions of allowed Bragg reflections. The curve at the bottom is the difference between the observed and calculated intensities in the same scale.

no big structural changes occur in the discharge-charge process. Compared to samples made using the solution method, samples made using the solid-state method have a smaller charging depth-dependent diffusion coefficient. In addition, for samples with a Li composition altered at the time of synthesis, samples with lower Li composition have larger chemical diffusion coefficients. Therefore, in the solid-state method, Li^+ can be considered to diffuse more easily in samples with lower Li composition. This may be one reason why samples with low Li composition made using the solid-state method have favorable battery properties.

3.4. Crystal structure and nuclear density analyses using powder neutron diffraction

In order to investigate why the battery properties of $Li_xNi_{0.8}Co_{0.2}O_2$ are dependent on the synthesis method and Li composition from the perspective of crystal structure, powder neutron diffraction measurements were taken and Rietveld analysis of the crystal structure was carried out. As an example, the crystal structure parameters of $Li_{0.994}Ni_{0.8}Co_{0.2}O_2$ obtained using the solid-state method are shown in Table 3 and their profile is shown in Fig. 7. In the crystal structure analysis, it was assumed that in the space group *R*-3*m*, Li was in the 3a site (0,0,0), a transition metal was in the 3b site (0,0,1/2), and oxygen was in the 6c site (0,0,*z*). Furthermore, cation mixing was considered, in which Ni^{2+}, which has nearly the same ionic radius as Li^+, partially occupies the 3a site and Li^+ partially occupies the 3b site. The analytical composition was used for the composition of each metallic constituent. The analysis was carried out treating the isotropic atom displacement parameter *B* as a variable to the greatest extent possible. Due to this, as shown in Fig. 7, the profiles of the calculated values and the measured values match well, and, as shown in Table 3, a small S value was obtained. For samples that correspond during the charge process, because the measured values and the calculated values using the same crystal structure model match, it was confirmed that the layered structure is maintained during the charge process. Furthermore, neutron diffraction measurements show that Li_2CO_3 exists in samples with excessive Li composition ($0.994 < x \leq 1.082$), and hence analysis was carried out with Li_2CO_3 (space group *C12/c1*) as phase 2. Table 4 indicates the amount of cation mixing obtained in the structural analysis and the rate of Li_2CO_3 relative to $Li_xNi_{0.8}Co_{0.2}O_2$. In Section 3.2, it was noted that excessive Li composition in $Li_xNi_{0.8}Co_{0.2}O_2$ decreases the battery properties. Considering this fact, we presume that the existence of Li_2CO_3 in samples with excessive Li composition is one factor that lowers the cycling performance. In addition, in samples with excessive Li composition, we observe a tendency for Li cation mixing at the 3b site to increase. It can be presumed that this is another factor in the decrease in the discharge capacity and cycling performance. Furthermore, no significant change in cation mixing was seen in samples that correspond during charging ($x < 0.965$). From these facts, it can be presumed that cation mixing takes place at

Table 4
Relationship between Li content, cation mixing of 3a and 3b site of $Li_xNi_{0.8}Co_{0.2}O_2$, and Li_2CO_3 ratio.

Synthetic method	Li content, *x*	Atom	Site	Site occupancy	Li_2CO_3
Solid-state method	0.530	Ni	3a	0.056(3)	
		Li	3b	0.03(1)	
	0.660	Ni	3a	0.051(2)	
		Li	3b	0.05(1)	
	0.756	Ni	3a	0.050(4)	
		Li	3b	0.02(2)	
	0.965	Ni	3a	0.075(3)	
		Li	3b	0.04(2)	
	0.994	Ni	3a	0.032(4)	
		Li	3b	0.026	
	1.041	Ni	3a	0.020(4)	0.029
		Li	3b	0.047	
	1.066	Ni	3a	0.052(4)	0.015
		Li	3b	0.112	
Solution method	0.438	Ni	3a	0.039(4)	
		Li	3b	0.03(1)	
	0.651	Ni	3a	0.031(2)	
		Li	3b	0.02(1)	
	0.880	Ni	3a	0.058(3)	
		Li	3b	0.02(1)	
	1.082	Ni	3a	0.038(4)	0.062
		Li	3b	0.091	

Table 5
Bond lengths (nm) of $Li_xNi_{0.8}Co_{0.2}O_2$ prepared by various synthetic methods.

Synthetic method	Li content, *x*	3a–6c	3b–6c
Solid-state method	0.530	2.121(1)	1.933(1)
	0.660	2.118(1)	1.940(1)
	0.756	2.125(1)	1.959(1)
	0.965	2.101(1)	1.963(1)
	0.994	2.108(1)	1.966(1)
	1.041	2.105(1)	1.961(1)
	1.066	2.103(1)	1.960(1)
Solution method	0.438	2.131(1)	1.922(1)
	0.651	2.124(1)	1.938(1)
	0.880	2.114(1)	1.960(1)
	1.082	2.091(1)	1.961(1)

Table 6
Distortion around 3b site, λ, σ^2, and bond valence sum of 3b site of $Li_xNi_{0.8}Co_{0.2}O_2$ prepared by various synthetic methods.

Synthetic method	Li content, *x*	Bond valence sum	λ	σ^2
Solid-state method	0.530	3.465	1.006	20.02
	0.660	3.358	1.006	19.79
	0.756	3.261	1.006	18.93
	0.965	3.174	1.004	14.06
	0.994	3.104	1.004	14.99
	1.041	3.107	1.005	15.65
	1.066	3.028	1.005	15.28
Solution method	0.438	3.562	1.007	22.88
	0.651	3.271	1.006	20.71
	0.880	3.257	1.005	16.78
	1.082	3.079	1.004	12.60

the time of synthesis and there are no significant changes in the charge–discharge process.

Table 5 shows bond lengths obtained through structural analysis. In materials with Li chemically removed ($x < 0.965$), for both synthesis methods the 3a–6c bond length increases and the 3b–6c bond length decreases. It can be presumed that one factor leading to this is the fact that when the Li composition decreases, Ni is oxidized and its ionic radius decreases. On the other hand, in samples with excessive Li composition, as the Li composition increases, the length of the 3a–6c bond decreases. In addition, it is clear that the 3a–6c bond length is longer in samples created using the solid-state method than in solution method samples. On the other hand, in samples with excessive Li composition, the 3a–6c bond length decreases as the Li composition increases. In addition, it is clear that the 3a–6c bond length is longer in samples created using the solid-state method than in solution method samples. Table 6 shows the bond valence sum (BVS) of the 3b site, quadratic elongation λ, and the bond angle variance σ^2 [28] of the (Ni, Co, Li)-0_6 octahedron, obtained through structural analysis. This corresponds to the tendency for the average valance of the 3b site to increase due to Li^+ desorption during charging. In addition, in samples with excessive Li composition, the BVS decreases. This can be presumed to be due to the fact that the average valence of the 3b site decreases due to an increase in Li at the 3b site, as shown in Table 4. Deforma-

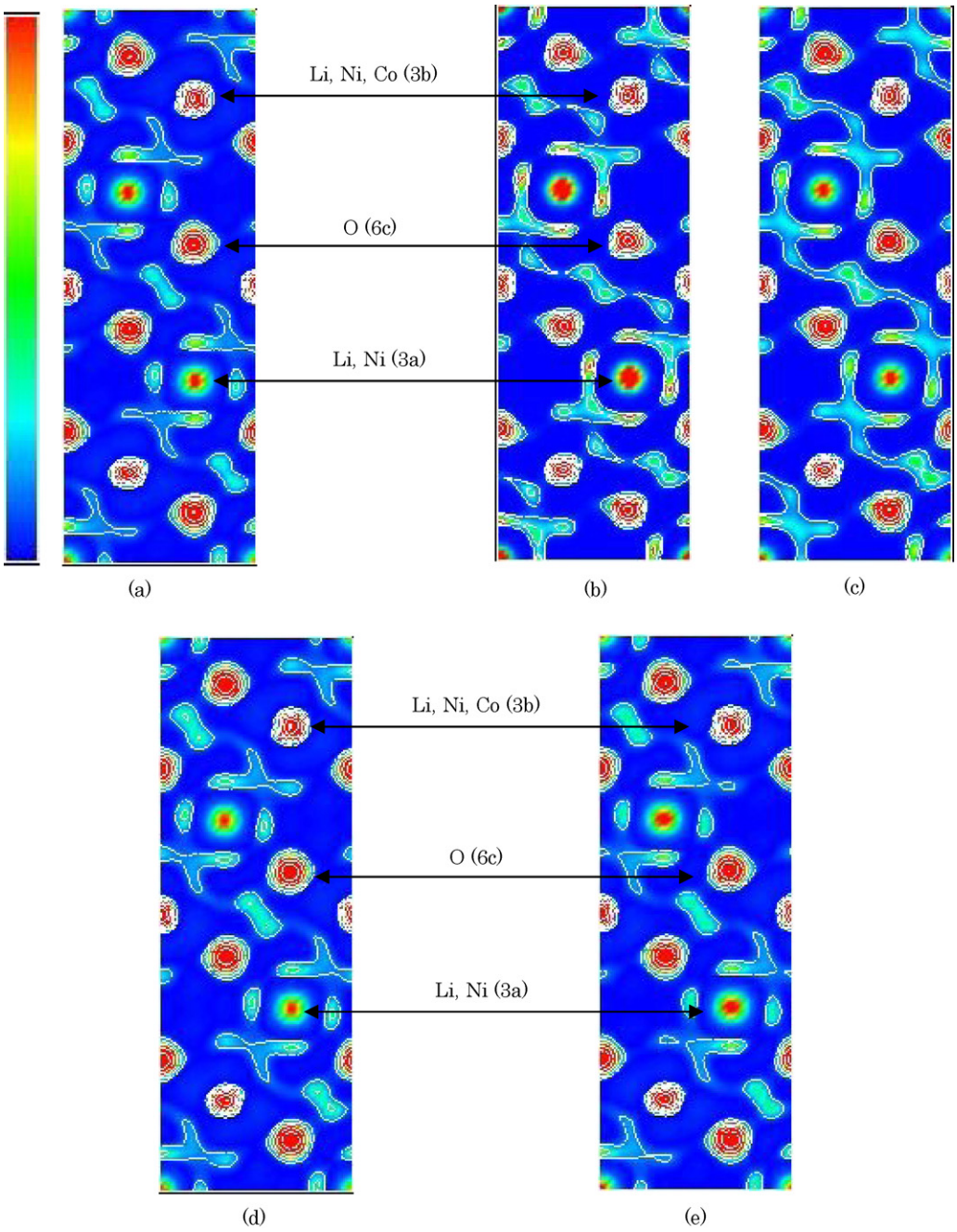

Fig. 8. Nuclear density images of $Li_xNi_{0.8}Co_{0.2}O_2$ (1 1 0) plane calculated by PRIMA. Contours are drawn from 0.5 to 2.58×10^{47} fm Å^{-3} with the interval of 0.5×3^n fm Å^{-3} (n; 0–100). (a) $x = 0.965$, $wR_F = 2.01\%$, (b) $x = 0.994$, $wR_F = 1.66\%$, (c) $x = 1.041$, $wR_F = 1.78\%$, (d) $x = 1.066$, $wR_F = 2.06\%$ (solid-state method), (e) $x = 1.082$, $wR_F = 1.86\%$ (solution method).

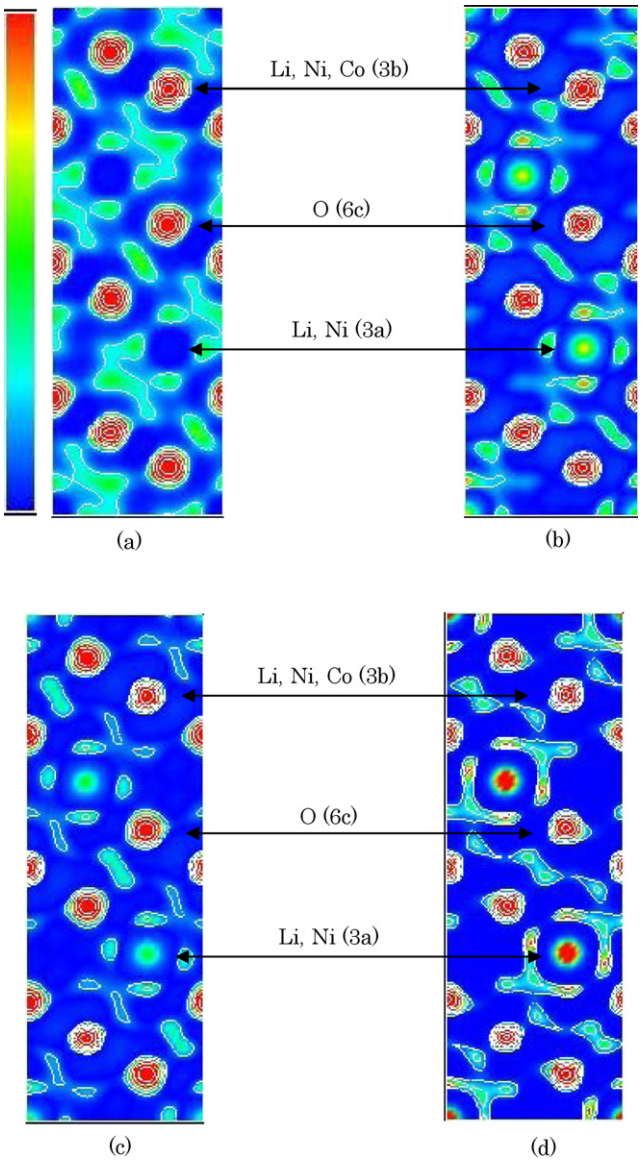

Fig. 9. Nuclear density images of delithiated $Li_xNi_{0.8}Co_{0.2}O_2$ (1 1 0) plane (solid-state method). Contours are drawn from 0.5 to 2.58 × 10^{47} fm Å^{-3} with the interval of 0.5 × 3^n fm Å^{-3} (n; 0–100). (a) x = 0.530, wR_F = 1.68%, (b) x = 0.660, wR_F = 1.61%, (c) x = 0.756, wR_F = 2.01%, (d) x = 0.994, wR_F = 1.66%.

tion due to quadratic elongation (λ) was not significant even when the Li composition was decreased. On the other hand, σ^2 increases when the Li composition is decreased. This indicates that although $Li_xNi_{0.8}Co_{0.2}O_2$ maintains its layered structure during the charge process, the area around the 3b site is distorted due to desorption of Li^+.

Based on the crystal structural analysis, we investigated the nuclear density distribution in the crystal using MEM. Fig. 8 shows the nuclear density distribution of the (1 1 0) plane for samples made with the solid-state method and Fig. 9 shows the nuclear density distribution of the (1 1 0) plane of a chemically delithiated $Li_{0.994}Ni_{0.8}Co_{0.2}O_2$ sample made by the same method.

As indicated above, changes in cation mixing were seen in samples for which the Li composition was changed at the time of synthesis. However, as the change was small, no large changes were observed in the nuclear density distribution at each site (Fig. 8). However, when chemical delithiation is carried out, the nuclear density of the 3a site decreases as the Li composition decreases, and no major changes were observed at the 3b and 6c sites. From this, it is understood that Li^+ desorption occurs at the 3a site during charging and that no major changes occur in cation mixing. It is clear that the host structure, the layered structure in other words, of $Li_xNi_{0.8}Co_{0.2}O_2$ made in this study was stable even during the charge process. In addition, in samples made using the solution method, the same tendency was seen as for the solid-state method, and no major differences were seen at each site based on different synthesis methods.

3.5. Electron density analysis using powder X-ray diffraction

In order to investigate bonding between each atom in $Li_xNi_{0.8}Co_{0.2}O_2$, crystal structural analysis was carried out using powder X-ray diffraction patterns, and electron density distributions were investigated using MEM. Fig. 10 shows the (1 1 0) plane electron density distribution obtained for a sample made using the solid-state method and Fig. 11 shows the (1 1 0) plane electron density distribution after chemical delithiation. From this, it can be presumed that decreases in the Li composition cause a decrease in the charge density of the 3b site and an increase in covalent bonding. Consequently, we suggest that not only the average ionic radius of the 3b site, but also the 3b–6c bonding characteristics influence the bond length. Furthermore, in Fig. 10(d), (e), in the sample range with excessive Li (x > 0.994), a tendency for the 3b–6c covalent bond to decrease as the Li composition decreases was observed. Furthermore, the 3a–6c covalent bond showed a greater increase for samples made with the solution method than for solid-state method samples, and it is clear that this corresponds to the decrease in the 3a–6c bond length found by Rietveld analysis of the neutron diffraction pattern. In addition, a similar tendency was observed for $Li_x(Mn,Co,Ni,M)O_2$ (M = Al, Ti, Fe), which has a layered structure [5,6].

3.6. The relationship between solid-state properties, crystal structure, and battery properties

An evaluation of battery performances shows that samples made with the solid-state method have better cycling performances than samples made with the solution method. Furthermore, in $Li_xNi_{0.8}Co_{0.2}O_2$ synthesized using the solid-state method, as the Li composition decreases, the initial discharge capacity decreases while the discharge capacity maintenance rate increases and the cycling performance improves. Whereas, no differences in the particle radius and particle shape due to the synthesis method could be seen. Therefore, the effect of particle morphology on the electrode properties due to the synthesis method is minimal. On the other hand, the powder neutron diffraction measurements of these samples showed that in the samples with an excessive Li composition, a small amount of Li_2CO_3 exists as an impurity. Furthermore, as the Li composition increases, Li^+ at the 3b site tends to increase. These facts may be the cause of the decrease in the discharge capacity and cycling performance of samples with the excessive Li composition. In the chemically delithiated samples with the corresponding charging process, there were no major changes in the cation mixing, and although there was distortion around the 3b site, it is clear that the layered structure was maintained. Whereas, the chemically delithiated samples are possibly different from the electrochemically charged samples. Therefore, we are now investigating the crystal structure of the electrochemically charged samples based on synchrotron

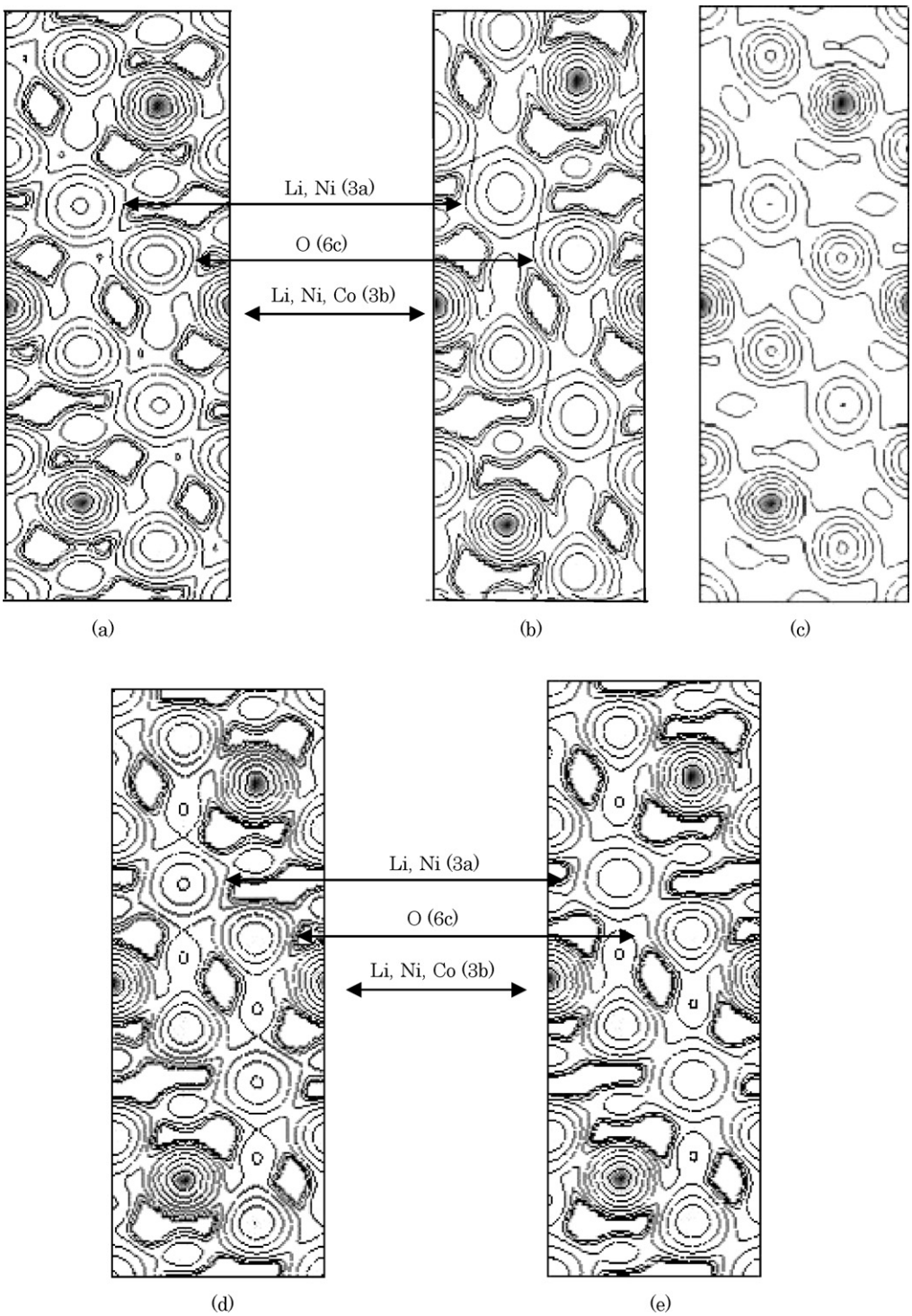

Fig. 10. Electron-density images of $Li_xNi_{0.8}Co_{0.2}O_2$ (1 1 0) plane calculated by PRIMA. Contours are drawn from 0.01 to 5.15×10^{45} e Å^{-3} with the interval of 0.01×3^n e Å^{-3} (n; 0–100). (a) $x = 0.965$, $wR_F = 1.65\%$, (b) $x = 0.994$, $wR_F = 1.88\%$, (c) $x = 1.041$, $wR_F = 2.01\%$, (d) $x = 1.066$, $wR_F = 1.54\%$ (solid-state method), and (e) $x = 1.082$, $wR_F = 1.63\%$ (solution method).

X-ray diffraction data. These results will be reported in the future.

As the Li composition decreases for both synthesis methods, the 3a–6c bond length increases and the 3b–6c bond length decreases. Furthermore, it was found that the 3a–6c bond length was longer for samples made using the solid-state method than for solution method samples. These results correspond to the electron density distribution obtained through MEM. Hence, it can be considered that the bonding between each metal and oxygen influences the crystal structure.

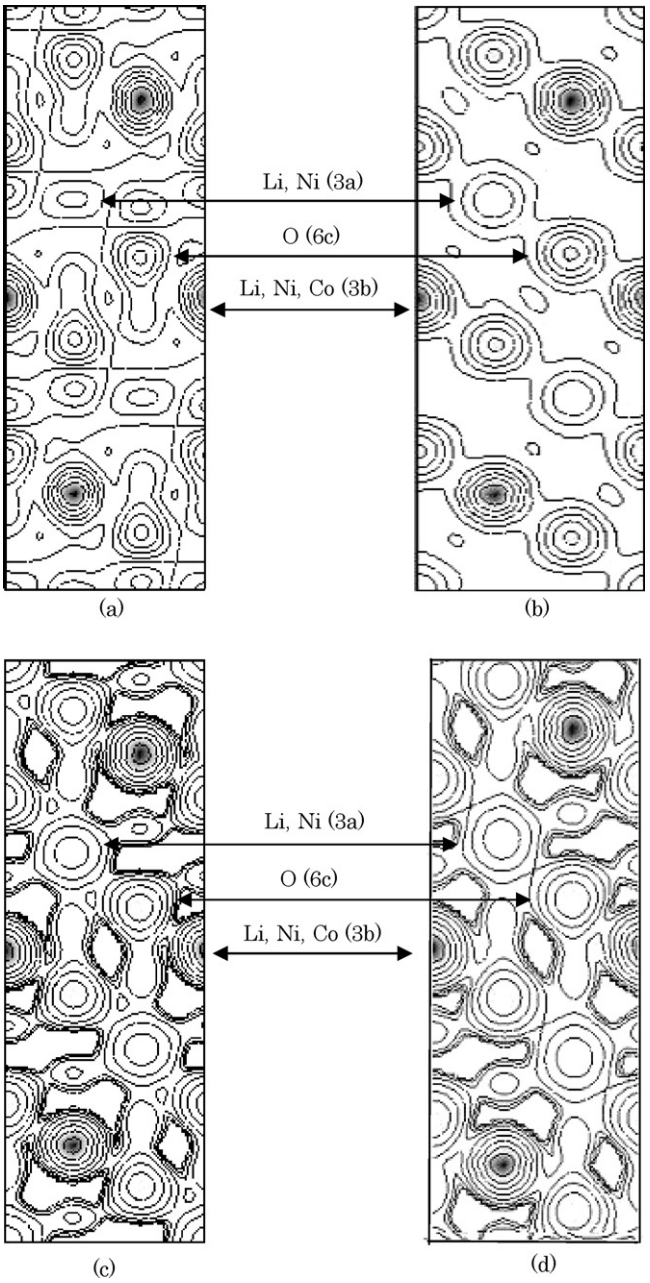

Fig. 11. Electron-density image of delithiated $Li_xNi_{0.8}Co_{0.2}O_2$ (1 1 0) plane calculated by PRIMA (solid-state method). Contours are drawn from 0.01 to 5.15×10^{45} e Å^{-3} with the interval of 0.01×3^n e Å^{-3} (n; 0–100). x = 0.530, wR_F = 1.68%, (b) x = 0.660, wR_F = 1.61%, (c) x = 0.756, wR_F = 2.01%, and (d) x = 0.994, wR_F = 1.88%.

4. Conclusions

The following points were obtained regarding $Li_xNi_{0.8}Co_{0.2}O_2$ synthesis methods and Li composition dependency.

(1) Charge–discharge cycle experiments show that samples made with the solid-state method have better cycling performances than samples made with the solution method. When the Li composition at the time of synthesis decreases, the initial discharge capacity decreases while the discharge capacity maintenance rate increases and the cycling performance improves.

(2) Investigations of the chemical diffusion coefficient demonstrate that Li^+ is more easily diffused in samples made with the solid-state method that have lower Li composition. This is one reason why samples made with the solid-state method with low Li composition have favorable battery performances.

(3) Powder neutron diffraction measurements show that a small amount of Li_2CO_3 exists in samples with excessive Li composition, which was not confirmed in X-ray diffraction measurements. In addition, in these samples an increasing tendency for Li^+ to exist at the 3b site was observed. These are factors leading to decreasing cycling performance in the same material.

(4) In samples that were chemically delithiated, irrespective of the synthesis method, as the Li composition decreases, the 3a–6c bond length increases and the 3b–6c bond length decreases. In addition, in samples with excessive Li composition, the 3a–6c bond length decreases.

(5) The nuclear density distribution of chemically delithiated samples suggests that there is no change in cation mixing even when charging and that the layered structure is maintained.

(6) The electron density distribution reveals a tendency for the 3b–6c covalent bond to increase as the Li composition at the time of synthesis decreases. Furthermore, samples with excessive Li composition show a tendency for the 3b–6c covalent bond to decrease. Compared to solid-state method samples, samples made with the solution method exhibit an increasing 3a–6c covalent bond, corresponding to the bond length found in neutron diffraction.

(7) The above points show that for $Li_xNi_{0.8}Co_{0.2}O_2$, the synthesis method and Li composition affect cation mixing and 3a–6c and 3b–6c bonding. This in turn influences the cycling performance and the structural stability of the host compounds.

Acknowledgements

We are indebted to Dr. K. Oyama and Mr. K. Nemoto (Tohoku University) for assisting with the powder neutron diffraction measurements at HERMES(JRR-3M). This work was partly supported by MEXT, HAITEKU (2005–2007).

References

[1] S.S. Shin, Y.K. Sun, K. Amine, J. Power Sources 112 (2002) 634.
[2] Y. Ito, Y. Idemoto, N. Koura, Electrochemistry 72 (2004) 20.
[3] Y. Idemoto, K. Konnno, K. Ui, N. Koura, Electrochemistry 73 (2005) 823.
[4] Y. Idemoto, T. Mochizuki, K. Ui, N. Koura, J. Electrochem. Soc. 153 (2006) A418.
[5] Y. Idemoto, T. Sakaya, N. Koura, Electrochemistry 74 (2006) 752.
[6] Y. Idemoto, T. Matsui, N. Koura, Electrochemistry 75 (2007) 791.
[7] D. Caurant, N. Baffier, B. Garcia, J.P. Pereira, Solid State Ionics 91 (1996) 45.
[8] C. Wang, X. Ma, L. Zhou, J. Cheng, J. Sun, Y. Zhou, Electrochim. Acta 52 (2007) 3022.
[9] Y.K. Sun, I.H. Oh, K.Y. Kim, J. Mater. Chem. 7 (1997) 1481.
[10] W. Tang, H. Kanoh, K. Ooi, J. Solid State Chem. 142 (1999) 19.
[11] K. Ohoyama, T. Kanouchi, K. Nemoto, M. Ohashi, T. Kajitani, Y. Yamaguchi, Jpn. J. Appl. Phys. 37 (1998) 3319.
[12] F. Izumi, T. Ikeda, Mater. Sci. Forum 321–324 (2000) 198.
[13] I.D. Brown, R.D. Shannon, Acta Crystallogr. A 29 (1973) 266.
[14] F. Izumi, R.A. Dilanian, Recent Research Developments in Physics, vol. 3, Transworld Research Network, Trivandrum, 2002, p. 699.
[15] F. Izumi, J. Cryst. Soc. Jpn. 44 (2002) 380.
[16] W. Weppner, R.A. Huggins, J. Electrochem. Soc. 124 (1977) 1569.
[17] Y. Gao, M.V. Yakovleva, W.B. Ebner, Electrochem. Solid-State Lett. 1 (1998) 117.
[18] T. Ohzuku, A. Ueda, M. Nagayama, Y. Iwakoshi, H. Komori, Electrochim. Acta. 38 (1993) 1159.
[19] Z. Wang, Y. Sun, L. Chen, X. Huang, J. Electrochem. Soc. 151 (2004) A914.
[20] Y. Idemoto, T. Matsui, Electrochemistry 75 (2007) 791.

[21] P.G. Bruce, A. Lisowska-Oleksjak, M.Y. Saidi, C.A. Vincent, Solid State Ionics 57 (1992) 353.
[22] L. Chen, J. Schoonman, Solid State Ionics 67 (1994) 17.
[23] K.M. Shajyu, G.V. Subba Tal, B.V.T. Chowdari, Electrochim. Acta 49 (2004) 1565.
[24] J.Y. Go, S.U. Pyun, H.C. Shin, J. Electroanal. Chem. 527 (2002) 93.
[25] L.A. Montoro, J.M. Rosolen, Electrochim. Acta 49 (2004) 3243.
[26] E. Deiss, Electrochim. Acta 47 (2002) 4027.
[27] G.G. Belmonte, Z. Pomerantz, J. Bisquert, J.P. Lellouche, A. Zaban, Electrochim. Acta 49 (2004) 3413.
[28] R. Keith, V.G. Gibbs, H.P. Ribbe, Science 172 (1970) 567.